PROBABILISTIC MAP BUILDING CONSIDERING SENSOR VISIBILITY

Kazuma Haraguchi, Jun Miura
Department of Computer-Controlled Mechanical Systems, Graduate School of Engineering, Osaka University
2-1 Yamadaoka, Suita, Osaka, Japan
haraguti@cv.mech.eng.osaka-u.ac.jp, jun@mech.eng.osaka-u.ac.jp

Nobutaka Shimada, Yoshiaki Shirai
Department of Computer Science Faculty of Science Engineering Ritsumeikan University
1-1-1 Nojihigashi, kusatsu, shiga, Japan
shimada@ci.ritsumei.ac.jp, shirai@i.ci.ritsumei.ac.jp

Keywords: Obstacle Map Generation, Bayes Theorem, Occlusion, Spatial Dependency, Visibility.

Abstract: This paper describes a method of probabilistic obstacle map building based on Bayesian estimation. Most active or passive obstacle sensors observe only the most frontal objects and any objects behind them are occluded. Since the observation of distant places includes large depth errors, conventional methods which does not consider the sensor occlusion often generate erroneous maps. We introduce a probabilistic observation model which determines the visible objects. We first estimate probabilistic visibility from the current viewpoint by a Markov chain model based on the knowledge of the average sizes of obstacles and free areas. Then the likelihood of the observations based on the probabilistic visibility are estimated and then the posterior probability of each map grid are updated by Bayesian update rule. Experimental results show that more precise map building can be bult by this method.

1 INTRODUCTION

The well known SLAM(Simultaneous Localization And Mapping)(Montemerlo and Thrun, 2002; Thrun et al., 2004; Grisetti et al., 2005) process could be divided in two parts: position localization using current observations and the current map, and the map update using the estimated position. This paper discusses the problem of the conventional map update methods, *sensor occlusion*, and proposes a novel updating method solving it.

The positions of landmarks and obstacles should be represented on the map for navigation(Thrun, 2002b). There are two representations available for them:

1. Feature point on the obstacle
2. Obstacle existence on small map grid.

Former representation requires feature identification and matching and the feature position is update when new observation is available(Suppes et al., 2001). Latter representation identifies the map grid from which the observation comes. Since laser range sensors, ultrasonic sensors and stereo image sensors can precisely control the direction of transmitting and receiving light or sound, the place from which observation comes is easy to identify. Thus we use the latter map representation here.

The obstacle sensor output always includes observation errors. For example flight time measurement of light or sound have errors caused by wave refraction, diffraction and multi-path reflection. Stereo image sensor also has correspondence failures of image features. These errors lead to large errors or ghost observations. Therefore the map building should be established in a probabilistic way based on a certain error distribution model.

Here we use a probabilistic occupancy grid map for the map representation, which stores the obstacle existence probability in each map grid. In this representation, the obstacle existence probability of each grid is updated by evaluating the likelihood of obtained observation for the grid and integrate it with its prior probability in the way of Bayesian estimation. While a generic solution of this map building formulation is solved by Markov Random Field (MRF)

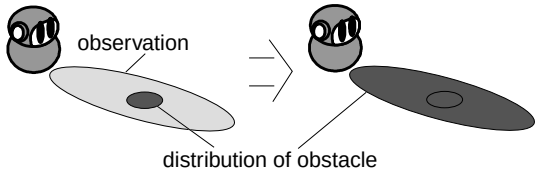

Figure 1: Result of update when the robot gets the observation of the obstacle of substantial margin of error.

(Rachlin et al., 2005), its computational cost is huge, especially in case of high grid resolution. Previous methods (Miura et al., 2002; Thrun, 2002a; Moravec, 1988) use the following assumptions for reduction of computation:

1. Observation obtained for each map grid is probabilistically independent (it depends on only the state (obstacle existence) of that grid).
2. Obstacle existence of each map grid is independent to each other.

Most obstacle sensors observe the most frontal objects and any objects behind them are occluded. Since such sensors having *sensor occlusion* characteristic does not satisfy the above assumption 1, the following serious problems are caused by forcedly using the assumption.

As shown in the left side picture of Figure 1, suppose that dark grey ellipsoidal region has higher probability of obstacle existence than the outside. Then suppose that the obstacle observation with large error (ex. distant observation with stereo vision) is obtained shown as the light grey region in the figure. In that situation, that observation probably comes from the most frontal part of the dark grey region. The assumption 1, however, the obstacle existence probability of each map grid is independently updated by integrating the observation and it is obviously overestimated. As a result everywhere distant from the current robot position tends to be estimated as obstacle in the map. Therefore the assumption 1 should be rejected.

In addition, the assumption 2 also leads to the other problems. If the obstacle existence in each map grid is independent, the probability of that a certain area is open as free-space is estimated as the product of the probability of each map grid. This leads to an obviously irrational result that more precise grid resolution is adopted, abruptly smaller becomes the free-space probability of the same area (in other words, the viewing field is more invisible due to occluding obstacles).

In real scenes, obstacles and free-spaces has a certain size. This points out the existence of co-occurrence between the adjacent grids, called *spatial continuity*. Since the co-occurrence becomes larger when the grid resolution is more precise, the free-space probability can be correctly estimated regardless of the grid resolution. Thus the assumption 2 also should be rejected.

Our map building method correctly considers sensor occlusion and spatial continuity. A certain obstacle is visible if and only if the space between the sensor and the obstacle is entirely open as free-space. Therefore we introduce a novel method of estimating *visibility* of the obstacle on each map grid by considering spatial continuity, and updating the obstacle existence probability with proper consideration of sensor occlusion.

2 MAP BUILDING CONSIDERING SENSOR VISIBILITY

2.1 Joint Probability of Adjacent Grids on Each Viewing Ray

We first divide the map grids into multiple viewing rays. The sensor observes the existence of obstacle on each ray. In this paper, we represent the viewing ray as the 4-connected digital line as shown in Figure 2. On each ray we consider the probabilistic grid state (whether obstacle exists on the grid or not) as a simple Markov chain. Thus each grid state can be represented as the joint probability of two grid states adjacent on each ray.

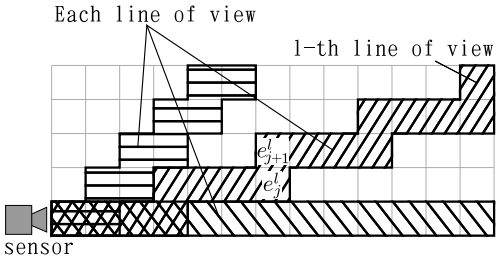

Figure 2: Approximated Lines of view.

We first estimate the joint probability of the jth and $j+1$th grid (the jth grid is nearer to the sensor) on a viewing ray (see Figure 2). Let $e^l_j = \left\{E^l_j, \bar{E}^l_j\right\}$ be the state of the jth grid on the lth ray (E:occupied by an obstacle, $\bar{E}$: not occupied), and $P(e^l_j, e^l_{j+1}|\mathbf{O})$ be the joint probability of the jth and $j+1$th grid under $\mathbf{O}$, the series of the previous observations. Then the joint probability after the latest observation $\mathbf{o}$ obtained

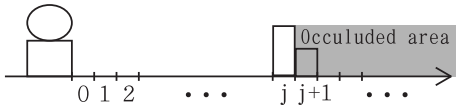

Figure 3: Occluded area behind the j-th grid.

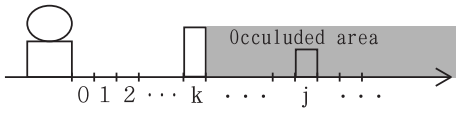

Figure 4: Occluded area behind the k-th grid.

is calculated as :

$$P(e^l_j, e^l_{j+1}|\mathbf{o}, \mathbf{O}) = \alpha^l P(o^l|e^l_j, e^l_{j+1}, \mathbf{O}) P(e^l_j, e^l_{j+1}|\mathbf{O}). \quad (1)$$

o^l, α^l, $P(e^l_j, e^l_{j+1}|\mathbf{O})$ and $P(o^l|e^l_j, e^l_{j+1}, \mathbf{O})$ respectively denote the observation on the ray l, a normalizing constant, the prior probability and the likelihood. The likelihood $P(o^l|e^l_j, e^l_{j+1}, \mathbf{O})$ should be calculated by considering the sensor visibility as the following section.

2.2 Likelihood Considering Sensor Visibility

Since an observation on the ray l, o^l, depends on grid states just on the the ray, the likelihood $P(o^l|e^l_j, e^l_{j+1}, \mathbf{O})$ is calculated as:

$$P(o^l|e^l_j, e^l_{j+1}, \mathbf{O}) = \sum_{\mathbf{m}^l \in \Omega^l} P(o^l|\mathbf{m}^l, e^l_j, e^l_{j+1}, \mathbf{O}) P(\mathbf{m}^l|e^l_j, e^l_{j+1}, \mathbf{O}) \quad (2)$$

where $\mathbf{m}^l$ denotes grid states on the ray l except e^l_j,e^l_{j+1}. The direct calculation of Eq. 2 requires huge summation of 2^{N_l} order, where N_l denotes the number of grids on the ray l.

Actually this calculation is drastically reduced by considering the sensor visibility. There exist four cases of the adjacent grid states: (E_j, E_{j+1}), $(E_j, \bar{E}_{j+1})$, $(\bar{E}_j, E_{j+1})$, $(\bar{E}_j, \bar{E}_{j+1})$. In (E_j, E_{j+1}) case (this means both the grid j and $j+1$ are occupied), since grid j occludes $j+1$ as shown in Figure 3, the likelihood $P(o^l|E^l_j, E^l_{j+1}, \mathbf{O})$ is no longer dependent on $j+1$, and then it is represented as

$$P(o^l|E^l_j, E^l_{j+1}, \mathbf{O}) = P(o^l|E^l_j, \mathbf{O}). \quad (3)$$

The above likelihood is acceptable only when grid j is visible from the sensor, namely whole grids between the sensor and grid j are empty. If not so, the most frontal occupied grid $k(< j)$ is observed (see Figure 4). Here, define an stochastic event F_k as follows:

$$F_k = \begin{cases} \bar{E}_0 & (k=0) \\ \bar{E}_0 \cap \bar{E}_1 \cap \cdots \cap \bar{E}_{k-1} \cap E_k & (k>0). \end{cases}$$

Since $F_0, \cdots, F_k$ are mutually exclusive events, the right-hand of Eq.3 is expanded as follows:

$$\begin{aligned} P(o^l|E^l_j, \mathbf{O}) &= \sum_{k=0}^{j} P(o^l|F^l_k, E^l_j, \mathbf{O}) P(F^l_k|E^l_j, \mathbf{O}) \\ &= \sum_{k=0}^{j} P(o^l|F^l_k) P(F^l_k|E^l_j, \mathbf{O}) \end{aligned} \quad (4)$$

because o^l is no longer dependent on any grid behind grid k nor the previous observations $\mathbf{O}$.

The likelihoods for the rest three cases $(E_j, \bar{E}_{j+1})$, $(\bar{E}_j, E_{j+1})$, $(\bar{E}_j, \bar{E}_{j+1})$, is represented as follows in the same considerations:

$$P(o^l|E^l_j, \bar{E}^l_{j+1}, \mathbf{O}) = \textstyle\sum_{k=0}^{j} P(o^l|F^l_k) P(F^l_k|E^l_j, \mathbf{O}) \quad (5)$$

$$\begin{aligned} P(o^l|\bar{E}^l_j, E^l_{j+1}, \mathbf{O}) = {} & \textstyle\sum_{k=0}^{j-1} P(o^l|F^l_k) P(F^l_k|\bar{E}^l_j, \mathbf{O}) \\ & + P(o^l|F^l_{j+1}) P(F^l_{j+1}|\mathbf{O}) \end{aligned} \quad (6)$$

$$\begin{aligned} P(o^l|\bar{E}^l_j, \bar{E}^l_{j+1}, \mathbf{O}) = {} & \textstyle\sum_{k=0}^{j-1} P(o^l|F^l_k) P(F^l_k|\bar{E}^l_j, \mathbf{O}) \\ & + \textstyle\sum_{k=j+1}^{\infty} P(o^l|F^l_k) P(F^l_k|\mathbf{O}). \end{aligned} \quad (7)$$

$P(o^l|F^l_k)$ in Eqs.(4)-(7) is a sensor kernel model which defines the measurement error distribution of the sensor observation. This is provided for each kind of sensor. These equations say that the likelihood of grid j and $j+1$ is contributed by grid k ahead grid j according to $P(F^l_k|E^l_j, \mathbf{O})$, $P(F^l_k|\bar{E}^l_j, \mathbf{O})$, $P(F^l_k|\mathbf{O})$, which mean conditional *visibilities* of grid k.

Since these visibilities are required to be estimated before the above likelihood calculations, they should be estimated by calculating the Markov chain because the actual grid states are not independent due to spatial continuity. The Markov chain is calculated based on the grid state probabilities (joint probability of e_j, and e_{j+1}) obtained in the previous time slice:

$$\begin{aligned} P(F^l_k|E^l_j, \mathbf{O}) = {} & P(\bar{E}^l_0|\bar{E}^l_1, \mathbf{O}) P(\bar{E}^l_1|\bar{E}^l_2, \mathbf{O}) P(\bar{E}^l_2|\bar{E}^l_3, \mathbf{O}) \\ & \cdots P(\bar{E}^l_{k-1}|E^l_k, \mathbf{O}) P(E^l_k|E^l_j, \mathbf{O}) \end{aligned} \quad (8)$$

$$\begin{aligned} P(F^l_k|\bar{E}^l_j, \mathbf{O}) = {} & P(\bar{E}^l_0|\bar{E}^l_1, \mathbf{O}) P(\bar{E}^l_1|\bar{E}^l_2, \mathbf{O}) P(\bar{E}^l_2|\bar{E}^l_3, \mathbf{O}) \\ & \cdots P(\bar{E}^l_{k-1}|E^l_k, \mathbf{O}) P(E^l_k|\bar{E}^l_j, \mathbf{O}) \end{aligned} \quad (9)$$

$$\begin{aligned} P(F^l_k|\mathbf{O}) = {} & P(\bar{E}^l_0|\bar{E}^l_1, \mathbf{O}) P(\bar{E}^l_1|\bar{E}^l_2, \mathbf{O}) P(\bar{E}^l_2|\bar{E}^l_3, \mathbf{O}) \\ & \cdots P(\bar{E}^l_{k-1}|E^l_k, \mathbf{O}) P(E^l_k|\mathbf{O}) \end{aligned} \quad (10)$$

where $P(E^l_k|\mathbf{O})$, $P(\bar{E}^l_{k-1}|E^l_k, \mathbf{O})$ and $P(\bar{E}^l_q|\bar{E}^l_{q+1}, \mathbf{O})$ $(0 \le q < k-1)$ are calculated as follows:

$$P(E^l_k|\mathbf{O}) = P(E^l_k, E^l_{k+1}|\mathbf{O}) + P(E^l_k, \bar{E}^l_{k+1}|\mathbf{O}) \quad (11)$$

$$P(\bar{E}^l_{k-1}|E^l_k, \mathbf{O}) = \frac{P(\bar{E}^l_{k-1}, E^l_k|\mathbf{O})}{P(E^l_{k-1}, E^l_k|\mathbf{O}) + P(\bar{E}^l_{k-1}, E^l_k|\mathbf{O})} \quad (12)$$

$$P(\bar{E}^l_q|\bar{E}^l_{q+1}, \mathbf{O}) = \frac{P(\bar{E}^l_q, \bar{E}^l_{q+1}|\mathbf{O})}{P(\bar{E}^l_q, \bar{E}^l_{q+1}|\mathbf{O}) + P(E^l_q, \bar{E}^l_{q+1}|\mathbf{O})}. \quad (13)$$

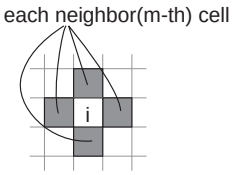

Figure 5: Adjacent grids.

$P(E_k^l|E_j^l,\mathbf{O})$ and $P(E_k^l|\bar{E}_j^l,\mathbf{O})$ are also obtained by calculating the Markov chain:

$$P(E_k^l,E_j^l|\mathbf{O}) = P(E_k^l|\mathbf{O})P(E_j^l|\mathbf{O}) + \alpha_{k,j}\prod_{q=k}^{j-1} c_{q,q+1}^l \quad (14)$$

$$P(E_k^l,\bar{E}_j^l|\mathbf{O}) = P(E_k^l|\mathbf{O})P(\bar{E}_j^l|\mathbf{O}) - \alpha_{k,j}\prod_{q=k}^{j-1} c_{q,q+1}^l \quad (15)$$

where

$$c_{q,q+1}^l = \frac{P(E_q^l,E_{q+1}^l|\mathbf{O}) - P(E_q^l|\mathbf{O})P(E_{q+1}^l|\mathbf{O})}{\sqrt{P(E_q^l|\mathbf{O})P(\bar{E}_q^l|\mathbf{O})P(E_{q+1}^l|\mathbf{O})P(\bar{E}_{q+1}^l|\mathbf{O})}} \quad (16)$$

$$\alpha_{k,j} = \sqrt{P(E_k^l|\mathbf{O})P(\bar{E}_k^l|\mathbf{O})P(E_j^l|\mathbf{O})P(\bar{E}_j^l|\mathbf{O})} \quad (17)$$

$c_{q,q+1}^l$ means correlation between the adjacent grid e_q^l and e_{q+1}^l. The grid visibilities are estimated from Eqs.(8)-(17), then the likelihoods considering sensor visibility, Eqs.(4)- (7), are calculated. Finally the posteriors, Eq.(1) is updated for each grid.

2.3 Posterior Update Across Viewing Rays

The grid posteriors for each viewing ray, estimated in the way of the previous section, conflict with the posteriors of the adjacent rays, because they actually have interactions across the rays and the independent update of each ray is just an approximation. True posteriors should satisfy the following two constraints: the first one is

$$\sum_{e_i,e_j\in\{E,\bar{E}\}} P(e_i,e_j) \equiv 1 \quad (18)$$

where grid i and j is adjacent, and the second one is

$$P(e_i) \equiv P(e_i,E_m) + P(e_i,\bar{E}_m) \quad (19)$$

for every grid m adjacent to grid j (see Figure 5). Therefore we estimate the true posteriors by least squares method under the constraints Eqs.(18),(19). The minimised error Δ^2 is written as

$$\Delta^2 = \sum_{i,j}\sum_{e_i,e_j}\left\{P^*(e_i,e_j) - P(e_i,e_j)\right\}^2 \quad (20)$$

where $P^*(e_i,e_j)$ is the conflicting posteriors, $P(e_i,e_j)$ is the estimated posteriors satisfying the constraints. This minimization is easily solved by Lagrange's method in low cost.

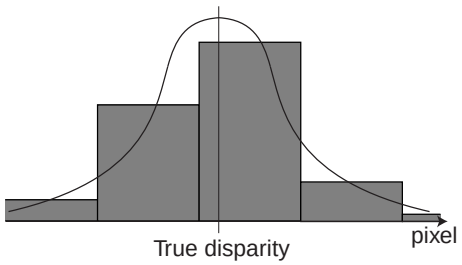

Figure 6: Probability density of the observation of the disparity.

3 EXPERIMENTS

3.1 Sensor Kernel Model of Stereo Vision

We compared a map building result for the simulation on a viewing ray and a real indoor scene using our method and a conventional method considering no sensor visibility nor spatial continuity.

In these experiments, we used edge-based stereo vision for observation of obstacles. Stereo vision provides depth information for each edge feature and it is well-known that the measurement error is inversely proportional to square of the depth. In addition erroneous feature matching can be found in a certain probability. Thus its sensor kernel model $P(o^l|F_k^l)$, required in Eqs.(4)- (7), are defined here as follows:

$$P(o^l|F_k^l) = P(T)P(o^l|F_k^l,T) + P(\bar{T})P(o^l|F_k^l,\bar{T}) \quad (21)$$

where o^l is the measured disparity for the viewing ray l, $P(T)$ (fixed to 0.8 in the following experiment, $P(T)+P(T\equiv 1)$) is the probability of obtaining a correct matching, $P(o^l|F_k^l,T)$ is a gaussian (see Figure 6), $P(o^l|F_k^l,\bar{T})$ is a uniform distribution over disparity range [0,60]. The obtained sensor kernel model $P(o^l|F_k^l)$ is shown in Figure 7.

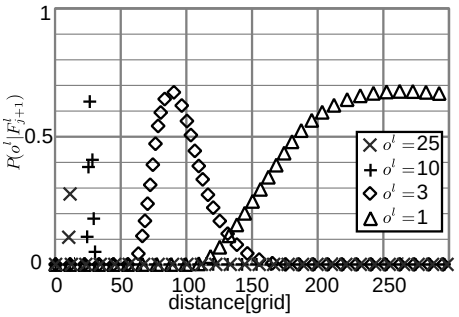

Figure 7: Observation model.

Our method updates the posteriors based on the likelihoods considering sensor visibility, Eqs.(4)-(7).

In the conventional method, we assume that state of each grid is independent from state of other grid as:

$$P(e_i^l|\mathbf{o},\mathbf{O}) = \frac{P(o_i^l|e_i^l,\mathbf{O})P(e_i^l|\mathbf{O})}{P(o_i^l|E_i^l,\mathbf{O})P(E_i^l|\mathbf{O}) + P(o_i^l|\bar{E}_i^l,\mathbf{O})P(\bar{E}_i^l|\mathbf{O})} \quad (22)$$

where o_i^l denotes the observation on ith grid and on lth ray. On this assumption we can calculate each grid indipendently. The following conventional likelihoods (Miura et al., 2002; Thrun, 2002a; Moravec, 1988) are adopted as a benchmark:

$$P(o_k^l = o_E|E_k^l) = P(o^l|F_k^l) \quad (23)$$
$$P(o_k^l = o_E|\bar{E}_k^l) = P(\bar{T}) \quad (24)$$
$$P(o_k^l = o_{\bar{E}}|E_k^l) = P(\bar{T}) \quad (25)$$
$$P(o_k^l = o_{\bar{E}}|\bar{E}_k^l) = P(T)\{1 - P(o^l|F_k^l,T)\}. \quad (26)$$

3.2 Posterior Update on a Viewing Ray

Our method of posterior update, of course, requires an initial prior distribution. In addition it requires an initial correlation parameter using for estimating the spatial continuity. In the following experiment, the initial prior $P(E_i)$ is uniformly set to 0.1 and the spatial correlation $c_{q,q+1}$ to 0.871 where the grid size is 5cm $\times$ 5cm These initial parameters are estimated based on average obstacle size (40cm $\times$ 40cm) in actual room scene samples.

Since the aim of this paper is to show the effectiveness of our posterior updating considering sensor visibility, we suppose that the exact robot position and orientation is known (NOT SLAM problem).

We compare our method with the convensional one without considering sensor visibility. We use three situations for the map update.

3.2.1 Case of Prior Probability of Uniform Distribution

Figure 8 shows the likelihood ratio and the posteriors when we take the observation (equivalent to the disparity of 10 pixels) in the uniform disribution. With considering sensor visibility, posteriors in the grid just behind the 30th grid is higher than that without considering visibility because we consider the average size of obstacles(equivalent to 40cm) in this experiment (see section 3.1).

3.2.2 Case of Uncertain Observation from Distant Place

In Figure 9 we establish that posteriors are estimated high from the 95th to the 110th grids after we obtain

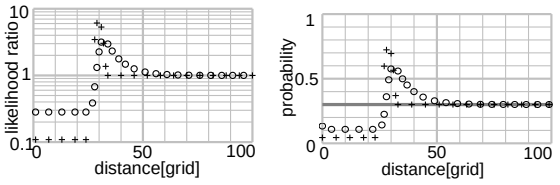

(a) Likelihood (b) Result of posterior update

Figure 8: Result of posterior update when the robot get the observation of the obstacle in the uniformly-distributed probablity area. "+" represents results of the conventional method. "◯" represents results of our method. The gray curve in (b) represents the prior probablity.

the observations. Figure 9 shows the likelihood and the posteriors when we get the observation (equivalent to the disparity of 3 pixels) with large error. Without considering visibility, posteriors in the range from the 80th to the 120th grid (equivalent to the disparity uncertainty of 3 pixels) becomes high. But we can not obtain the information in the range from the 90th to the 120th grid because we obtain the observation with the error which is larger than distribution of obstacles. For this reason with considering visibility, posteriors in the range from the 90th to the 120th grid does not change as Figure 9(b). On the other hand, in front of the range we can obtain the information that the obstacles does not exist. For this reason both methods show that posterior probability of obstacles existence becomes low in front of the range.

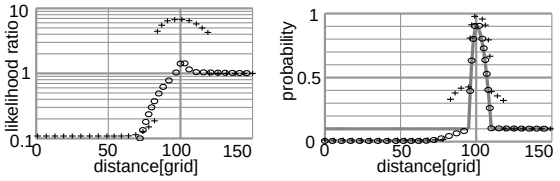

(a) Likelihood (b) Result of posterior update

Figure 9: Result of posterior update when the robot get the observation of the obstacle in the uniformly-distributed probablity area. "+" represents results of the conventional method. "◯" represents results of our method. The gray curve in (b) represents the prior probablity.

3.2.3 Case of Failure Observation for Occluded Area

In Figure 10 we establish that we obtain the failure observation for an occluded area when existence of obstacle is obvious. The error of this observation is about from the 200th to the 560th grid (equivalent to the disparity of 1 pixel). But it is highly possible that

the observation is failure because obstacle existence about the 100th grid is already know. With considering sensor visibility, the failure observation is automatically detected and the posteriors kept unchanged.

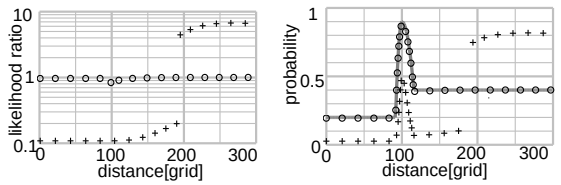

(a) Likelihood (b) Result of posterior update

Figure 10: Result of posterior update when the robot get the observation of the obstacle in the uniformly-distributed probablity area. "+" represents results of the conventional method. "◯" represents results of our method. The gray curve in (b) represents the prior probablity.

3.3 Result of Map Building

Next we show the result of map building for an actual room as shown in Figure 11. The mobile robot moved in the room observing obstacles with stereo cameras, starting from *A* point in Figure 11 via *B*, *C*, *B*, *D* through the grey line in the figure, and finally arrived at *B* point.

Figure 12 shows a view captured by the left camera. Figure 12(a) is a view from *A* point, and Figure 12(b) is another view from *B* point. We compared the built map of our method (Figure 14) to that of the conventional one (Figure 13). Sub-figure (a) and (b) of each figure shows the temporary map when the robot reached to *B* point via *A*, *B*, *C* and *D* point via *A*, *B*, *C*, *B* respectively, and sub-figure (c) shows the final map after the robot arrived at *B* point. Our method and the conventional method show the significantly difference at the circular region labelled *X*. The conventional method once estimate *X* as 'free-space' clearly when the robot was close to *X* (Figure

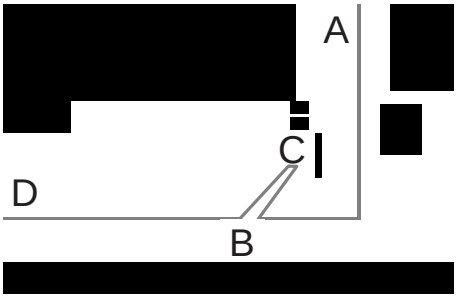

Figure 11: Rough map of obstacles.

(a) From A in Figure 11 (b) From D in Figure 11

Figure 12: Robot's view.

13(a)). When the robot re-observed *X* region from farther point, however, the detail information of *X* was missing and estimated as 'obstacle' rather than free-space due to the erroneous stereo observation from far point. (Figure 13(b),(c)). In contrast, our method correctly estimated the free-space in *X* without compromise due to the erroneous observation from far point (Figure 14(a),(b),(c)).

The process time for one update was about 1800ms on a PC with Athlon X2 4400+ CPU and 2GB memories.

4 CONCLUSIONS

We introduced a probabilistic observation model properly considering the sensor visibility. Based on estimating probabilistic visibility of each grid from the current viewpoint, likelihoods considering sensor visibility are estimated and then the posteriors of each map grid are updated by Bayesian update rule. For estimating grid visibility, Markov chain calculation based on spatial continuity is employed based on the knowledge of the average sizes of obstacles and free areas.

This paper concentrates the aim on showing the proof of concept of the probabilistic update considering sensor visibility and spatial continuity. For application to the real robot navigation, SLAM framework is necessary. In addition there are moving objects like human and semi-static objects like chairs or doors in the real indoor scene. The expansion to SLAM and environments with movable objects is the future works.

(a) At B via A, B, C

(b) At D via A, B, C, B

(c) At B via A, B, C, B, D

Figure 13: Result of map update without considering visibility and spatial dependencies.

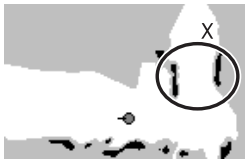

(a) At B via A, B, C

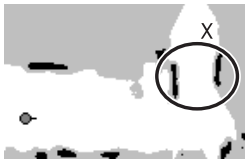

(b) At D via A, B, C, B

(c) At B via A, B, C, B, D

Figure 14: Result of map update considering visibility and spatial dependencies.

REFERENCES

Grisetti, G., Stachniss, C., and Burgard, W. (2005). Improving Grid-based SLAM with Rao-Blackwellized Particle Filters by Adaptive Proposals and Selective Resampling. In *Proc. of the IEEE International Conference on Robotics and Automation (ICRA)*, pages 2443–2448.

Miura, J., Negishi, Y., and Shirai, Y. (2002). Mobile Robot Map Generation by Integrationg Omnidirectional Stereo and Laser Range Finder. In *Proc. of the IEEE/RSJ Int. Conf. on Intelligent Robots and Systems (IROS)*, pages 250–255.

Montemerlo, M. and Thrun, S. (2002). FastSLAM 2.0: An Improved Particle Filtering Algorithm for Simultaneous Localization and Mapping that Provably Converges.

Moravec, H. P. (1988). Sensor fusion in certainty grids for mobile robots. In *AI Magazine, Summer*, pages 61–74.

Rachlin, Y., Dolan, J., and Khosla, P. (2005). Efficient mapping through exploitation of spatial dependencies. In *Proc. of the IEEE/RSJ Int. Conf. on Intelligent Robots and Systems (IROS)*, pages 3117–3122.

Suppes, A., Suhling, F., and Hötter, M. (2001). Robust Obstacle Detection from Stereoscopic Image Sequences Using Kalman Filtering. In *DAGM-Symposium*, pages 385–391.

Thrun, S. (2002a). Learning occupancy grids with forward sensor models. In *Autonomous Robots*.

Thrun, S. (2002b). Robotic Mapping: A Survey. In Lakemeyer, G. and Nebel, B., editors, *Exploring Artificial Intelligence in the New Millenium*. Morgan Kaufmann.

Thrun, S., Montemerlo, M., Koller, D., Wegbreit, B., Nieto, J., and Nebot, E. (2004). FastSLAM: An Efficient Solution to the Simultaneous Localization And Mapping Problem with Unknown Data Association. *Journal of Machine Learning Research*.